This document is the Accepted Manuscript version of a Published Work that appeared in final form in The Journal of Organic Chemistry, copyright © American Chemical Society after peer review and technical editing by the publisher. To access the final edited and published work see https://doi.org/10.1021/acs.joc.2c00617

Intermolecular Hydrogen-bond Assisted Solid-state Dual Emission Molecules with Mechanical Force-induced Enhanced Emission

Xiaohui Wang, Jianyu Zhang, Xiaoyu Mao, Yiwei Liu, Ruikuan Li, Jie Bai, Jun Zhang, Carl Redshaw, Xing Feng, Ben Zhong Tang**

Guangdong Provincial Key Laboratory of Information Photonics Technology, School of Material and Energy, Guangdong University of Technology, Guangzhou 510006, P. R. China

Department of Chemistry, Hong Kong Branch of Chinese National Engineering Research Center for Tissue Restoration and Reconstruction and Institute for Advanced Study, The Hong Kong University of Science and Technology, Kowloon, Hong Kong 999077, China.

School of Materials and Chemical Engineering, Anhui Jianzhu University, Hefei, 230601, P. R. China.

Department of Chemistry, University of Hull, Cottingham Road, Hull, Yorkshire HU6 7RX, UK.

Guangdong Provincial Key Laboratory of Luminescence from Molecular Aggregates (South China University of Technology), Guangzhou 510640, P. R. China.

Shenzhen Institute of Aggregate Science and Technology, School of Science and Engineering, The Chinese University of Hong Kong, Shenzhen 518172, China; AIE Institute, Guangzhou 510530, P. R. China.

KEYWORDS: Pyrene, chemical intermediate, hydrogen-bonds, blue emitter, force-induced enhanced emission

ABSTRACT: The presence of hydrogen bonds plays a crucial role not only in the life sciences, but also endows fantastic physical/chemical properties on molecules, which helps realize their high-tech applications. This work presents an efficient strategy to achieve highly efficient solid-state dual emission blue emitters with mechanical force-induced enhanced emission properties via intermolecular hydrogen-bonds via novel pyrene-based intermediates, namely 1,3,6,8-tetrabromo-2,7-dihydroxypyrene (**1**) and 1,3,6,8-tetrabromo-2- hydroxypyrene (**2**) prepared *via* hydroxylation and bromination of pyrene in high yield. Moreover, further use of a classical Pd-catalyzed coupling reaction affords new pyrene-based luminescent materials **3-5**, which display high thermal stability (in range from 336-447 ^{o}C), blue emission (< 463 nm) with high quantum yield in solution. Interestingly, with the mono-substituted hydroxyl (OH)/methoxyl (OMe) group located at the 2-position of pyrene, the compounds **4a** and **5** display an exciting dual emission with mechanical force-induced enhanced emission properties, due to the presence of several hydrogen bond interactions. Moreover, this series of compounds exhibits a number of advantages, for example deeper blue emission with narrower FWHM, a larger steric effect, and higher hydrophilicity. Thus, these novel bromopyrene intermediates and related pyrene-based luminescent materials will serve as a new platform to further explore novel organic solid-state luminescent materials for potential application in organic electronics, bioimaging, and chemsensors etc.

1. Introduction

Hydrogen bonds (H-bonds) are ubiquitous and play a crucial role in sustaining our life forms,[1] chemical reactions, [2] molecular engineering etc. [3] Molecules containing H-bonds have been widely designed for manipulating optical/electronic behavior, controlling molecular conformations, and molecular packing in order to realize their high-tech applications.[4,5]

Pyrene is a well-known structural core produced from the residue of the destructive distillation of coal tar,[6,7] and has been widely applied in various applications, [8,9,10,11,12] due to its excellent blue fluorescent properties and high charge carrier mobility. Pyrene containing alkylamide units are known to display fluorescent ferroelectric properties coupled with electron transport properties via intermolecular H-bonding and π-stacking interactions,[13] Araki *et al*. reported that amide-substituted pyrenes exhibit piezochromic luminescence via hydrogen-bond-directed assemblies.[14] Both examples indicated that the presence of H-bonds in pyrenes can result in interesting photophysical properties. However, due to limited synthetic strategies, hydrophilic pyrene-based intermediates/molecules are rare.

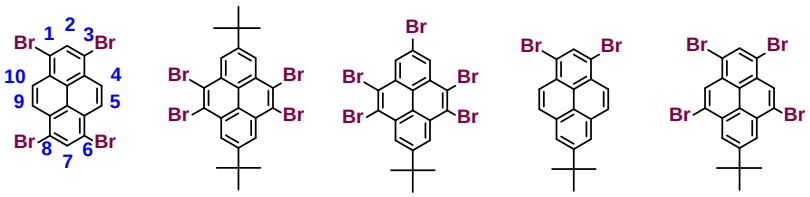

Scheme 1. Reported bromopyrene intermediates.[7,15,16]

Chemical intermediates are key building blocks in the manufacture of essential chemical compounds widely used in the chemical industry, medical applications, as well as in scientific research. The discovery of new intermediates has opened up many new research avenues and has led to a revolution in materials science and technological innovation. However, reports on efficient approaches for constructing pyrene-based new intermediates from chemical by-products are scant.[17]

Generally, the differentiated electronic structures of pyrene at the active sites (the 1-, 3-, 6- and 8-positions), the K-region (the 4-, 5-, 9- and 10-positions), or the node plane (the 2- and 7-positions) leads to pyrene derivatives with differing physical and chemical properties.[15] Thus, much effort has been devoted to developing novel pyrene-based precursors using optimized

synthetic procedures (Scheme 1 and Scheme S1), which have attracted immense interest in both industrial and academic communities. Among them, pyrenes containing reactive bromo substituents play a significant role in organic synthesis, and are key precursors for the preparation of various C-functionalized pyrene-based organic products obtained by metal-catalyzed cross-coupling reactions. On the other hand, pyrene can also be utilized in oxidation methods [18, 19, 20] and umpolung methods [21, 22] to access chemical intermediates that allow for further cross coupling and lithiation reactions, and the products are employed for various applications, such as organic light-emitting diodes (OLEDs), organic field-effect transistors (OFETs) [23] and chemosensors, etc.[24, 25, 26]

Since the classical intermediate 1,3,6,8-tetrabromopyrene was synthesized in 1937,[27] *via* a facile bromination reaction between pyrene and bromine (Br_2), there are now more than 1900 compounds of 1,3,6,8-substituted pyrenes that have been synthesized by Pd-catalysed coupling reactions, and their cutting-edge applications have also been explored over the past few decades. [7,10] Yamato *et al*. reported a direct synthetic method at the K-region (the 4,5,9,10-positions) of pyrene,[28] or both at the activated sites (1- and 3-positions) and the K-region (5- and 9-positions) by using a sterically bulky *tert*-butyl group as a protective group at the 2- or 7-positions, via an iron-catalyzed bromination reaction.[29] In addition, the difference in substituent positions at the pyrene core can strongly affect the optical properties, e.g. the 4,5,9,10-tetrakis substituted pyrenes exhibited a blue-shifted emission with a maximum band at 441 nm compared to the 1,3,6,8- tetrakis substituted pyrenes ($\lambda_{max\ em}$ = 496 nm in CH_2Cl_2).[28] Moreover, a non-doped OLED device displayed pure-blue electroluminescence (EL) emission at 468 nm using aggregation-induced emission luminogens (AIEgens), with 1,3,5,9-tetra(4-(1,2,2-triphenylvinyl)phenyl) pyrene as an emitter,[30] while for 1,3,6,8-tetra(4-(1,2,2-triphenylvinyl)phenyl)pyrene, the maximum EL

emission was located at 488 nm.[31] Up to now, about 12 types of milestone bromo-containing pyrene-based intermediates have been designed and synthesized, which are opening up many possibilities in terms of new pyrene-based opto-electronic functional materials for practical applications.[15, 16]

Theoretically, the active sites can preferentially undergo electrophilic aromatic substitution (S_{EAr}) reactions, and the substituents at the 2- and 7-positions only slightly affect the electronic communication with the pyrene core, leading to "pyrene-like" photophysical behaviour.[15] Thus, our group presented a new dual fluorescence emitter by decorating the 2- and 7-positions of pyrene using blue and yellow aggregation-induced emission units.[24] Previously, Marder *et al*. reported a new precursor, namely 2,7-dihydroxypyrene (**Py-2OH**), where small steric, hydrophilic hydroxyl groups (-OH) as substituents were introduced at the 2,7-positions of pyrene, increasing the hydrophilic capacity, and offering wider possibilities to functionalize the pyrene-based intermediates for the manufacture of organic fluorophores.[32] If the 2,7-dihydroxypyrene is brominated, do electrophilic reactions still occur at the 1-, 3-, 6- and 8-positions of pyrene? Moreover, what kind of emission behavior would be shown when the 2,7- and 1-, 3-, 6- and 8-positions of pyrene have been substituted simultaneously? Thus, this article presents an efficient approach to achieve new pyrene-based intermediates, with active groups not only at the 2,7-positions of pyrene, but also at the 1-, 3-, 6- and 8-positions, which can further be involved in a Suzuki coupling reaction to afford new star-shaped organic emitters. Interestingly, the presence of the -OH group located at the 2-/2,7-positions can strengthen the intra-/intermolecular interactions, leading to pyrene-based derivatives that have relatively weak fluorescence in the crystal, but display remarkable mechanically force-induced enhanced emission properties during the grinding process. Furthermore, such pyrene-based emitters can undergo a substitution reaction at the 2-/2,7-

positions for the construction of highly efficient solid-state dual-emission fluorescent materials. These studies open a new avenue for the preparation of novel pyrene-based functional materials for high-tech applications, such as organic electronics, chemsensors, and bioimaging.

3. Results and discussion

3.1 Synthesis and Characterization.

According to the synthetic route in Scheme 2, firstly, considering the hydrophilic properties of the precursor **Py-2OH**, acetic anhydride was selected as the reactive solvent, and the bromination between **Py-2OH** with bromine afforded a yellow unidentifiable compound. Thus, we repeated the classical reaction conditions following the literature, *i.e*. bromination of **Py-2OH** with bromine in nitrobenzene at 120^{o}C. A light-green product was achieved (91 %) (due to low solubility, the ^{1}H NMR spectrum could not be obtained), which by HRMS had a molecular peak at m/z^{+} = 548.6986. Similarly, bromination of **Py-OH** in nitrobenzene at 120^{o}C afforded a brown product in a yield of 92%, and the charge-mass ratio (m/z^{+}) is 532.7036. Both HRMS indicated that the intermediates 1,3,6,8-tetrabromo-2,7-dihydroxypyrene (**1**) and 1,3,6,8-tetrabromo-2-hydroxypyrene (**2**) were successfully synthesized.

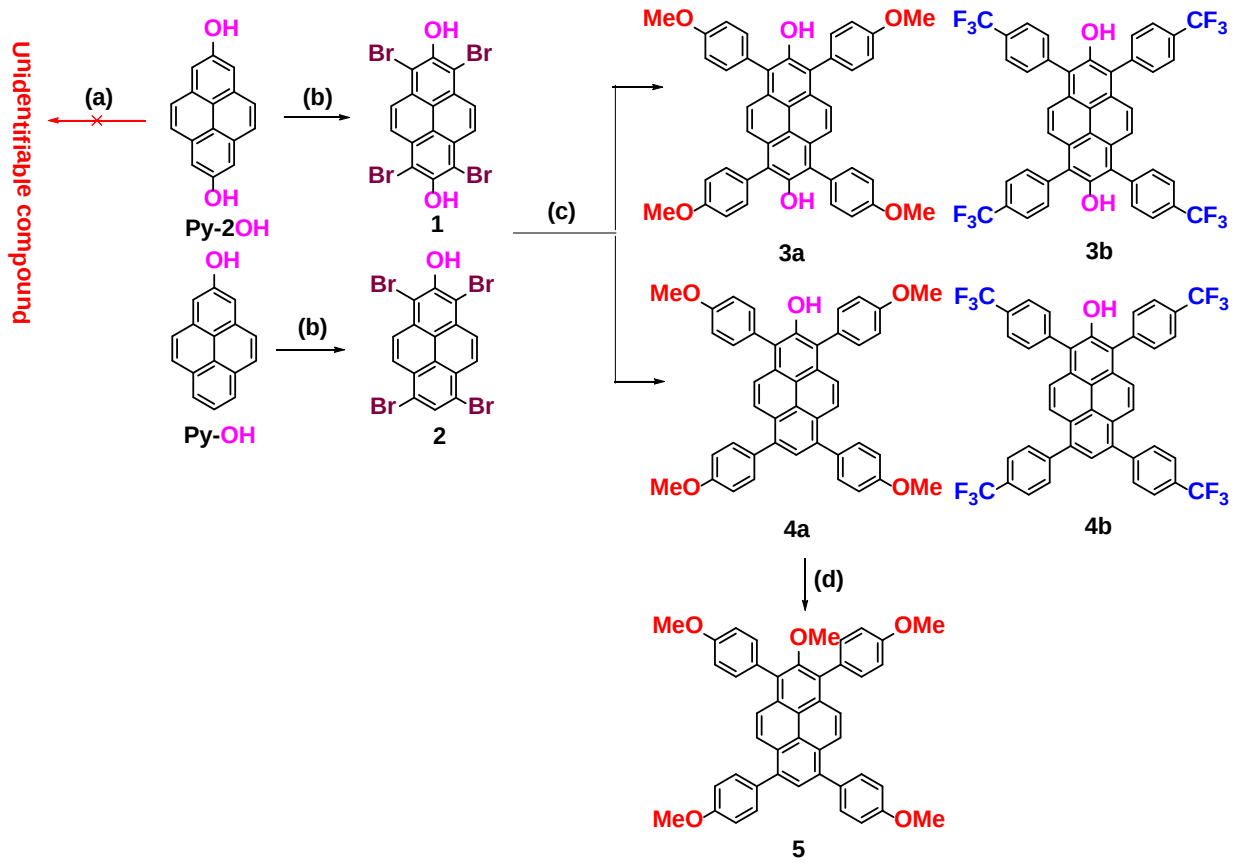

Scheme 2. Synthetic route to the new pyrene-based bromopyrene intermediates **1** and **2** by bromination of Py-2OH or Py-OH, and the corresponding novel tetrakis-arylsubstituted pyrenes **3** and **4** by a Suzuki coupling reaction. (a) liquid bromine, acetic anhydride, 120°C, 24 h, (b) bromine, nitrobenzene, 120°C, 24h, (c) R-C_6H_4-$B(OH)_2$, (R = OMe or CF_3), $Pd(PPh_3)_4$, K_2CO_3, toluene, ethanol, H_2O, 90°C, 24h, (d) CH_3I, CH_3CN, K_2CO_3, reflux.

Furthermore, a Suzuki-Miyaura coupling reaction between the bromopyrene intermediates (**1** and **2**) and the corresponding arylboronic acids with a stoichiometric ratio of 1:6 afforded 1,3,6,8-tetrakisaryl substituted-2,7-dihydroxypyrenes (**3a** and **3b**) or 1,3,6,8-tetrakisary substituted-2-hydroxypyrenes (**4a** and **4b**), respectively. To further confirm the activity of the -OH group at the 2-position, we conducted a methylation of compound **4a** with CH_3I to achieve a light-yellow

compound 1,3,6,8-tetrakis-(4-methoxylphenyl)-2-methoxyl pyrene (**5**) in 70% yield. All compounds were fully characterized by ^{1}H /^{13}C NMR spectra, HRMS, and single-crystal X-ray diffraction analysis. The decomposition temperature is in range from 336-447 ^{o}C with weight loss less than 5%. In addition, the 1,3,6,8-tetrakisary substituted-2,7-dihydroxypyrenes **3**-**4** are not easily oxidized to the corresponding pyrene-2,7-diones in solution.

As expected, this new pyrene system exhibited several advantages: (1) the presence of the -OH group increases the hydrophilic property of the pyrene derivatives, leading to enhanced solubility not only in common solvents, like dichloromethane (5 mg/mL), chloroform (10 mg/mL) and tetrahydrofuran (THF) (3mg/mL), but also larger polarity solvents, such as ethyl acetate (3mg/mL), *N*,*N*-dimethylformamide (4mg/mL), acetone (3mg/mL) etc.; (2) it offers an effective strategy to functionalize pyrene at both the 1,3,6,8-positions and 2,7-positions, thereby offering a possible route for introducing multi-functional groups and the construction of advanced optical materials, leading to highly desirable photophysical behavior; (3) the multi-positioned substituents at the pyrene core open up a new approach for constructing novel pyrene-based functional materials for multiple potential applications as organic light-emitting diodes, chemosensors, biomarkers etc.

3.2 Photophysical properties

The UV-vis absorption and emission spectra for compounds **3-5** were measured in dilute THF ($\sim 10^{-5}$ M) and are presented in Figure 1; the key parameters are listed in Table 1. The compounds exhibit two prominent absorption bands in the UV region (250-300 nm) and in the visible region (350-425 nm) with appreciable molar absorption coefficients (ε) of 20000-50000 M^{-1} cm^{-1}. As the number of -OH groups increase in the order **5** < **4** < **3**, then the molar absorption coefficients of the long-wavelength absorption band decrease from 51400 to 25600 M^{-1} cm^{-1}. The TD-DFT

calculations indicated that the longer wavelength absorption band is assigned to the $S_1 \leftarrow S_0$ and $S_2 \leftarrow S_0$ transitions, and the shorter wavelength absorption bands are attributable to the $S_3 \leftarrow S_0$ and $S_4 \leftarrow S_0$ transitions, respectively. For example, symmetrical **3** display a clear $S_1 \leftarrow S_0$ transition, in accordance with the weak absorption peak at 413 nm for **3a** and 415 nm for **3b**, respectively. Compared to the symmetrical compounds **3,** the unsymmetrical **4** and **5** show a slight red-shifted absorption peak (< 10 nm) with larger molar absorption coefficients (ε), which may be attributed to the disrupted electronic communication.[33] Although the -OH group was replaced by a methoxy group, compound **5** shows a similar absorption band to **4a**, which indicates that the small size of the substituent group at the 2,7-positions has only a slight effect on the electronic transition, due to the node plane passing through the 2,7-positions.[34] In addition, the electronic effect of the terminal group has a limited effect on the absorption band, which is agreement with our previous reports.[24, 25]

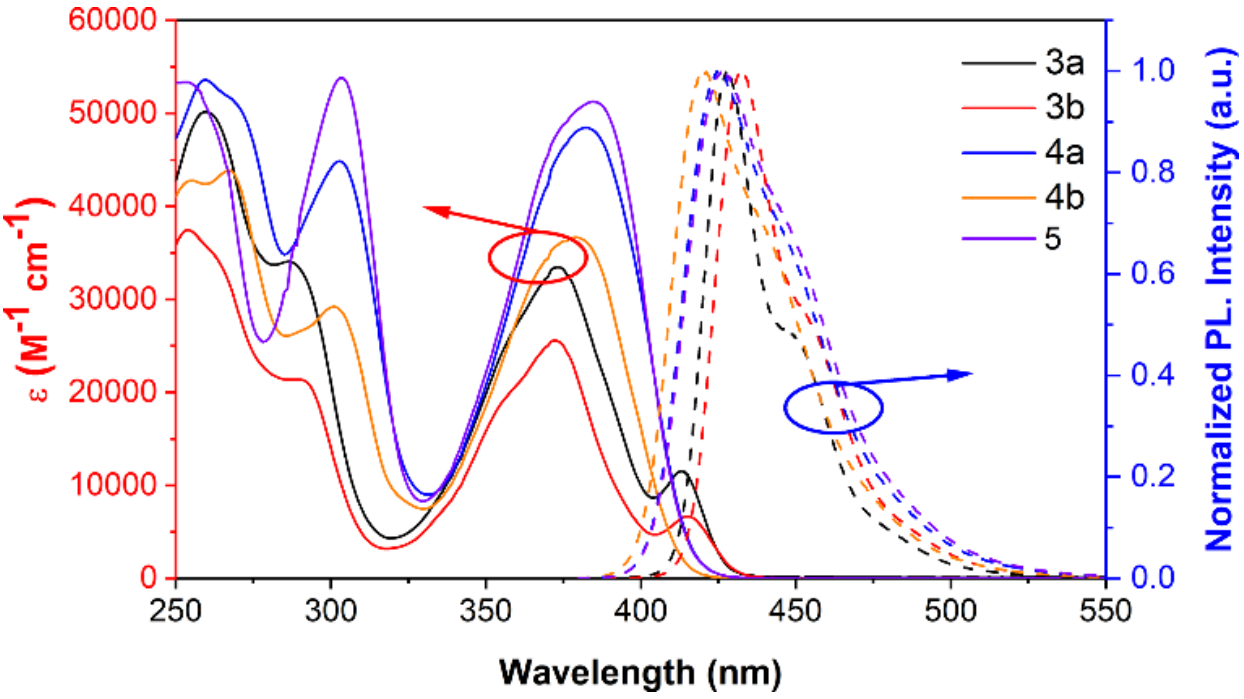

Figure 1. UV-vis and emission spectra of the pyrene-based derivatives **3**, **4** and **5** in THF solution (10^{-5} M).

Table 1. The photophysical properties of five new pyrene-based blue derivatives **3**, **4** and **5**.

	Transition	λ, nm (ε, M^{-1} cm^{-1})[a]	$\lambda_{maxPL,}$ (nm)	Φ_f[b]	τ, (ns)	LUMO (eV)[c]	HOMO (eV)[c]	Eg (eV)[c]
3a	$S_1 \leftarrow S_0$ $S_2 \leftarrow S_0$	413 (11600) 373 (33500)	428 (solns) 454, 500 (crystal) 456 (grinding)	0.53 (solns) 0.04 (crystal) 0.02 (grinding)	7.82 (solns) 1.43 (crystal, 454 nm) 2.40 (crystal 500 nm) 2.11 (grinding)	-1.63	-5.09	3.46
3b	$S_1 \leftarrow S_0$ $S_2 \leftarrow S_0$	415 (6600) 372 (25600)	432 (solns) 446 (crystal) 444 (grinding)	0.56 (solns) 0.04 (crystal) 0.04 (grinding)	9.71(solns) 4.13 (crystal) 3.14 (grinding)	-2.48	-5.97	3.49
4a	$S_1 \leftarrow S_0$[c]	382 (48500)	425 (solns) 463 (crystal) 460 (grinding)	0.63 (solns) 0.07 (crystal) 0.11 (grinding)	2.92(solns) 1.21 (crystal) 1.20 (grinding)	-1.65	-5.06	3.40
4b	$S_1 \leftarrow S_0$[c]	379 (36700)	420 (solns) 444 (crystal) 442 (grinding)	0.58 (solns) 0.24 (crystal) 0.12 (grinding)	6.65 (solns) 2.87 (crystal) 3.53 (grinding)	-2.54	-5.97	3.43
5	$S_1 \leftarrow S_0$[c]	385 (51400)	426 (solns) 446, 555 (crystal) 458, 555 (grinding)	0.83 (solns) 0.75 (crystal) 0.86 (grinding)	1.94 (solns) 1.51 (crystal, 446 nm) 7.29 (crystal 555 nm) 1.58 (grinding)	-1.70	-5.03	3.33

[a)] Maximum absorption wavelength measured in THF solution at room temperature. [b)] Measured in air. [c)] TD-DFT (B3LYP/6-311G(d,p)) calculations. [c)] Not possible to assign separate $S_1 \leftarrow S_0$ and $S_2 \leftarrow$S0 absorptions.

Upon excitation, the compounds **3-5** emit deep blue emission in dilute THF, with a maximum emission peak at 428 nm (**3a**), 432 nm (**3b**), 425 nm (**4a**), 420 nm (**4b**) and 426 nm (**5**) respectively.

The compounds **3** and **4** have slightly blue shifted emission (~5 nm) with a narrower full width at half maximum (FWHM) (< 55 nm), which may be due to the presence of the -OH (-OMe) group located at the 2,7-positions of pyrene, which can restrict the rotation of the terminal substituent group, leading to a rigid molecular scaffold (Table S6). The fluorescence quantum yields (Φ_f) of these compounds in THF solution were found to vary from 0.53-0.83. Otherwise, the fluorescence of the five compounds remains almost unchanged (< 10 nm) as the solvent polarity increasing from cyclohexane to DMSO (Figures S35~39 and Table S8).

3.3 Single-crystal X-ray diffraction analysis. Suitable single crystals of the five compounds for X-ray diffraction analysis were cultivated from a mixture of $CHCl_3$ and hexane solvents by slow evaporation at room temperature. Compounds **3a**, **3b**, **4a** and **5** crystallized in the monoclinic configuration, and the unit cell contains four molecules, respectively; the crystal unit cell of **4b** belongs to the triclinic system and contains one molecule. Otherwise, the hydroxy group in **4a** and **4b** are disordered between the 2- and 7-positions with an occupancy ratio 0.5:0.5 for the oxygen atom, respectively. Despite the small size of the -OH group at the 2,7-positions or the 2-position of pyrene, the adjacent groups can still influence the spatial structure of the -OH group. The bond angles (∠O-C-C) are in range 114.9 ^{o} to 123.0 ^{o}, with C-O bond distances of 1.306 – 1.432 Å in the crystals **3** and **4** (Table S2). It seems that the length of the C-O bond is shorter than a typical C-O bond.[35] In turn, larger dihedral angles (59.79-87.28^{o}) between the 4-methoxyphenyl group (or 4-trifluorophenyl) and the pyrene core are observed (Table S3). Moreover, both dihedral angles of crystal **3** are larger than found in 1,3,6,8-tetraaryl pyrenes between the pyrene and the four terminal moieties,[36-39] due to the steric effect of the hydroxyl group (-OH) at the 2,7-positions of pyrene. In crystal **5**, with the methoxy group at the 2-position, the dihedral angles between the 4-methoxyphenyl group at 1,3-positions and the pyrene core are in range 66.67 ^{o} to 88.62^{o}, which is

larger than for the 4-methoxyphenyl group at the 6,8-positions where no substituent was located at the 7-position of pyrene. Thus, the -OH or -OMe group at the 2-/2,7-positions can efficiently affect the adjacent groups via a steric effect.

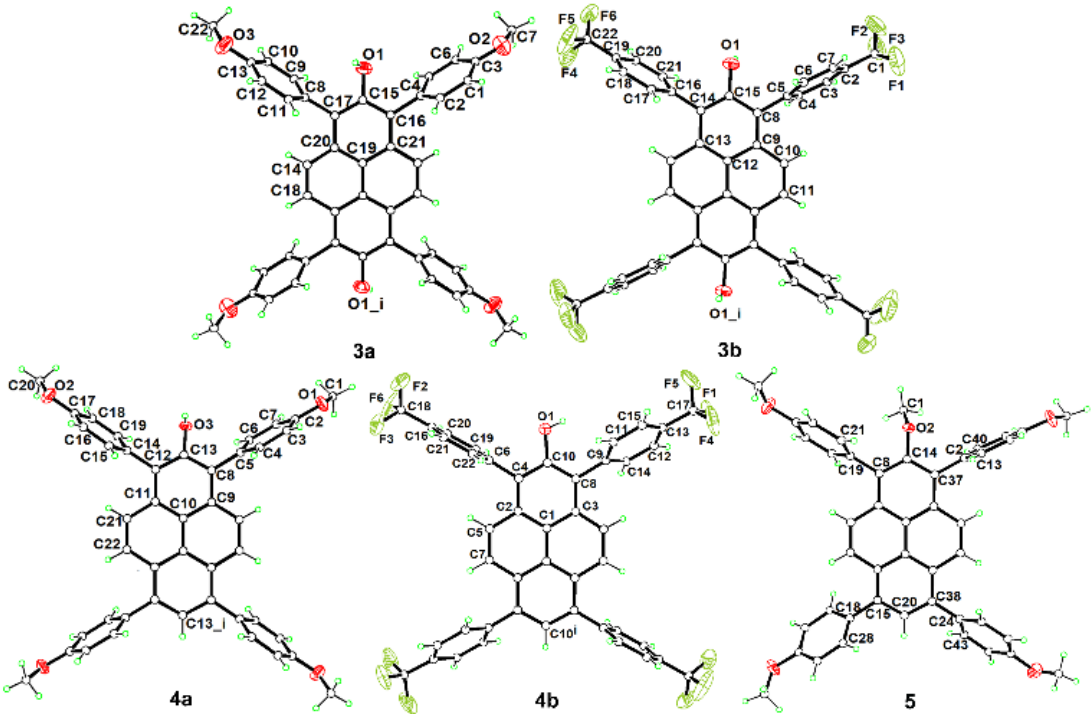

Figure 2. X-Ray structures of the pyrene derivatives **3-5**.

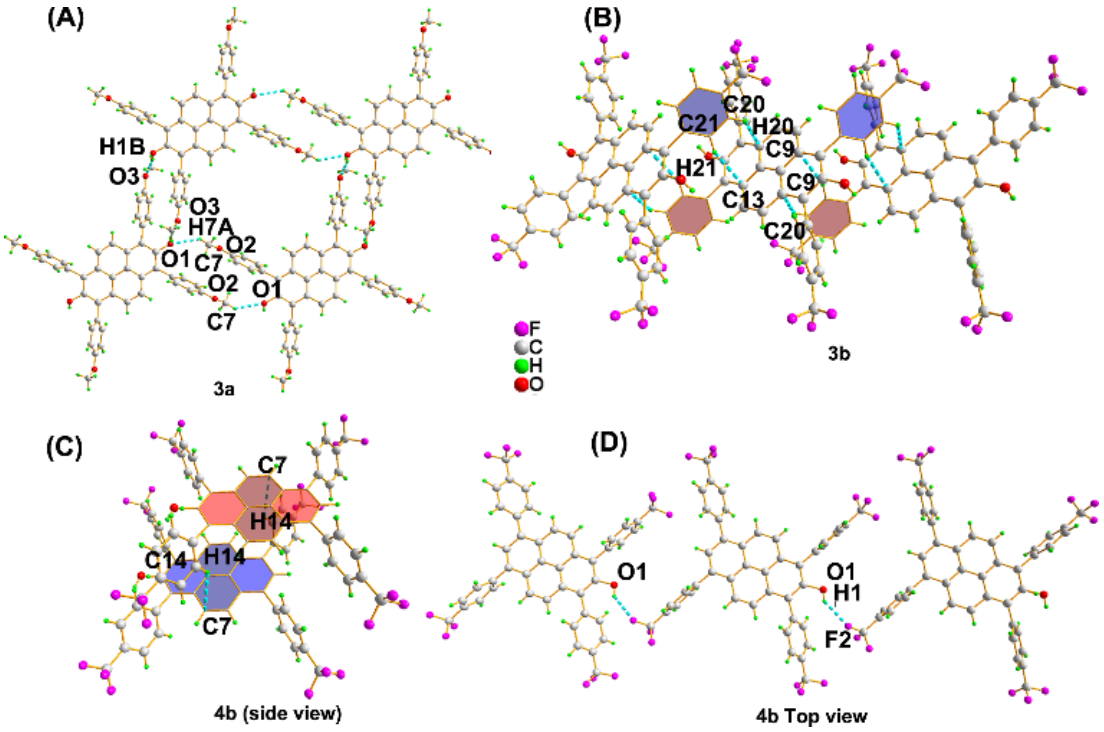

Figure 3. The packing structure of (A) crystal **3a**, (B) **3b**, (C) and (D) **4b** formed by weak intermolecular interactions.

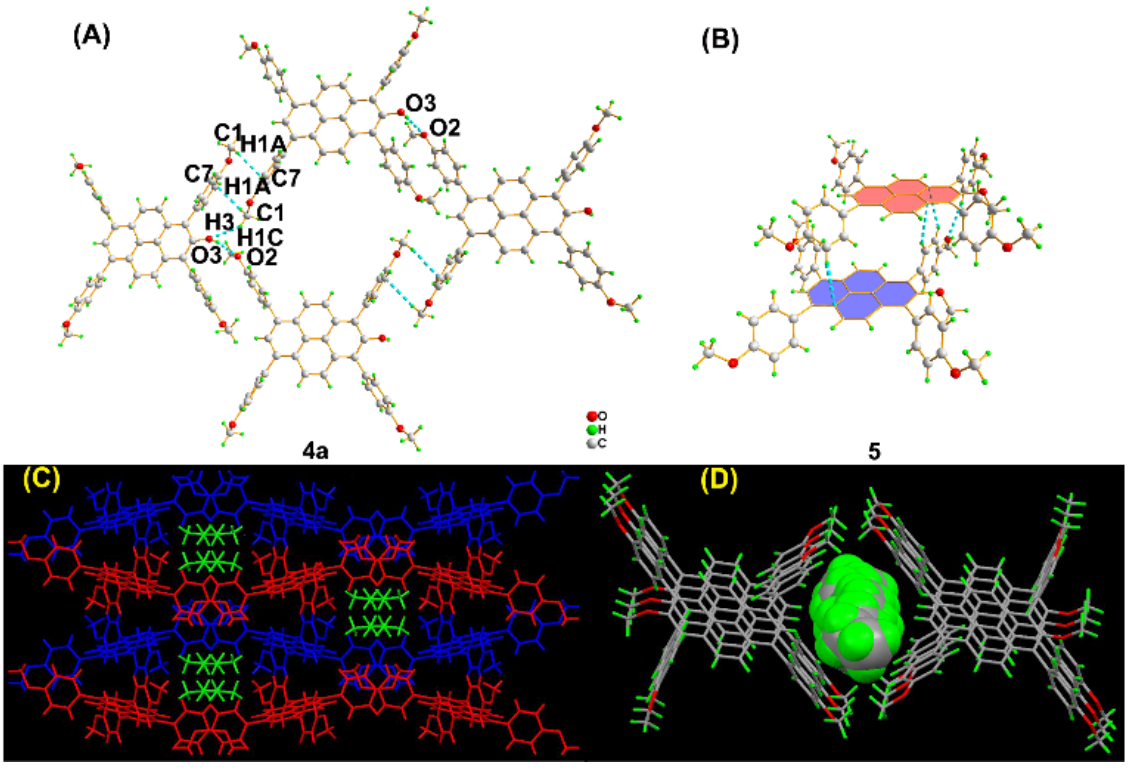

Figure 4. The packing structure of (A) and (C) crystal **4a**, (B) and (D) crystal **5** by weak intermolecular interactions.

The crystal structures for **3a**, **3b** and **4b** are presented in Figures 2 and 3. As shown in Figure 3(A), the molecule **3a** is connected with neighboring pyrenes via π-π stacking interactions of the terminal phenyl ring and several weak hydrogen bonds (C-H···O or C-H···F) to form 2D-molecular frameworks (Figures S27-S28). It is noteworthy that the length of the hydrogen bond between the -OH group and the methoxy group is 2.002 Å, which is an extremely short H-bond,[40] implying that the proton can transfer from the -OH to the adjacent -OMe group, leading to a strong charge-assisted hydrogen bond.[41,42] While the crystal **3b** exhibits a herringbone structure via several C-H···π interactions with distances of 2.854-2.879 Å. The centroid-to-centroid distance of two neighboring pyrenes is 8.039 Å. However, the crystal **4b** possesses face-to-face π-π stacking at a distance of 4.196 Å, which may be due to the stereoscopic effect of the -OH group at the 2-position and leads to the large dihedral angle between the 4-trifluorophenyl units and pyrene, which is conducive to restraining the π···π stacking interactions. In addition, the H atom on each -OH group participates in O-H···F interactions with a distance of 2.366 Å.

In the crystal **4a**, the 4-methoxyphenyl groups are involved in slipped π-π stacking interactions with a distance of 8.756 Å, and the compound is also self-assembled into a 2D honeycombed architecture as in **3a**, where disordered hexane molecules were captured in the interlayer. The -OH group at the 2-position of pyrene is connected with the methoxy group of the adjacent pyrene *via* a hydrogen bond (O3-H3···O2 = 2.035 Å). In addition, the molecules of **4a** arrange into a nano-scale molecular cavity *via* π-π stacking between the phenyl rings and several groups of C-H···O interactions, and the size of the cavity is larger than in **3a**. This may be due to just one -OH group

at the 2-position of pyrene in **4a**, which leads to a relatively weak intermolecular interaction. Thus, the -OH group at the 2-/2,7-positons can not only increase the steric effect, but also can contribute to the enhancement of the intermolecular interactions in the solid state.

On the other hand, when the -OH group was replaced by a methoxy group in crystal **5**, the packing structure displays slipped face-to-face π-π stacking along the *b*-axis at 4.626 Å. Interestingly, the self-assembled molecular tube is also filled up by disordered hexane molecules. Clearly, the π-π stacking plays a dominant role in arranging the crystal pattern. Thus, the presence of -OH groups can strengthen the inter/intramolecular interactions, to achieve different crystal packing, and may even lead to highly desirable photophysical behavior in the solid state.

3.4 Mechanical Force-induced enhanced emission. Generally, the molecular packing pattern plays a significant role on the emission behavior in the aggregation state.[43,44] Due to the large planar molecular structure of the pyrene core, which prefers to form a dimer or trimer via π-π stacking interactions, a large red-shifted emission is observed. In this case, the crystals of **3a** display a lighter blue emission under UV irradiation (λ_{ex} = 365 nm), and the emission spectra show a dual emission with the maximum emission at 454 nm with a shoulder peak at 500 nm, with Commission International Eclairage (CIE) coordinates of (0.1935, 0.2978). The crystals of **3b** emit deep blue emission with a maximum emission peak at 446 nm with CIE coordinates of (0.1534, 0.0609), and both **3a** and **3b** exhibit a low quantum yield (Φ_f) of *ca*. 0.04. The compounds **4a** and **4b** exhibit a relatively intense blue emission with maximum emission peaks at 463 nm (CIE: x=0.1504, y=0.1918) and 444 nm (CIE: x=0.1519, y=0.0877**)** in the crystal state and their Φ_f are 0.07 and 0.24, respectively. On replacing the -OH group by an -OMe group, the emission of compound **5** shows a dual emission with the maximum emission peak at 446 nm with a weak shoulder peak at 555 nm (CIE: x=0.1866, y=0.1782), and the Φ_f (0.75) is higher than **4a**, indicating

that the presence of the -OH group at the 2-/2,7-positions of pyrene would strength the intermolecular interactions between the adjacent molecules, leading to a deceased quantum yield. In addition, the fluorescence lifetime was measured for evaluating the electronic transition in the excitation state. As shown in Figure S40 and Table 1, the fluorescence lifetime (τ) of compounds **3**-**5** are higher in solution than in the solid state. Moreover, the fluorescence lifetime of the dual emission peaks at 454 nm and 500 nm for compound **3a** are 1.43 ns and 2.40 ns, and dual emission peaks at 500 nm for **3a** and 555 nm for compound **5** are 1.51 ns and 7.29 ns, respectively, and both shoulder emission peak are originating from the singlet transition, and the former may contribute to the charge-transfer emission, and the latter could be attributed to excimer or ground-state dimers, which is very common in pyrene or pyrene derivatives.[38]

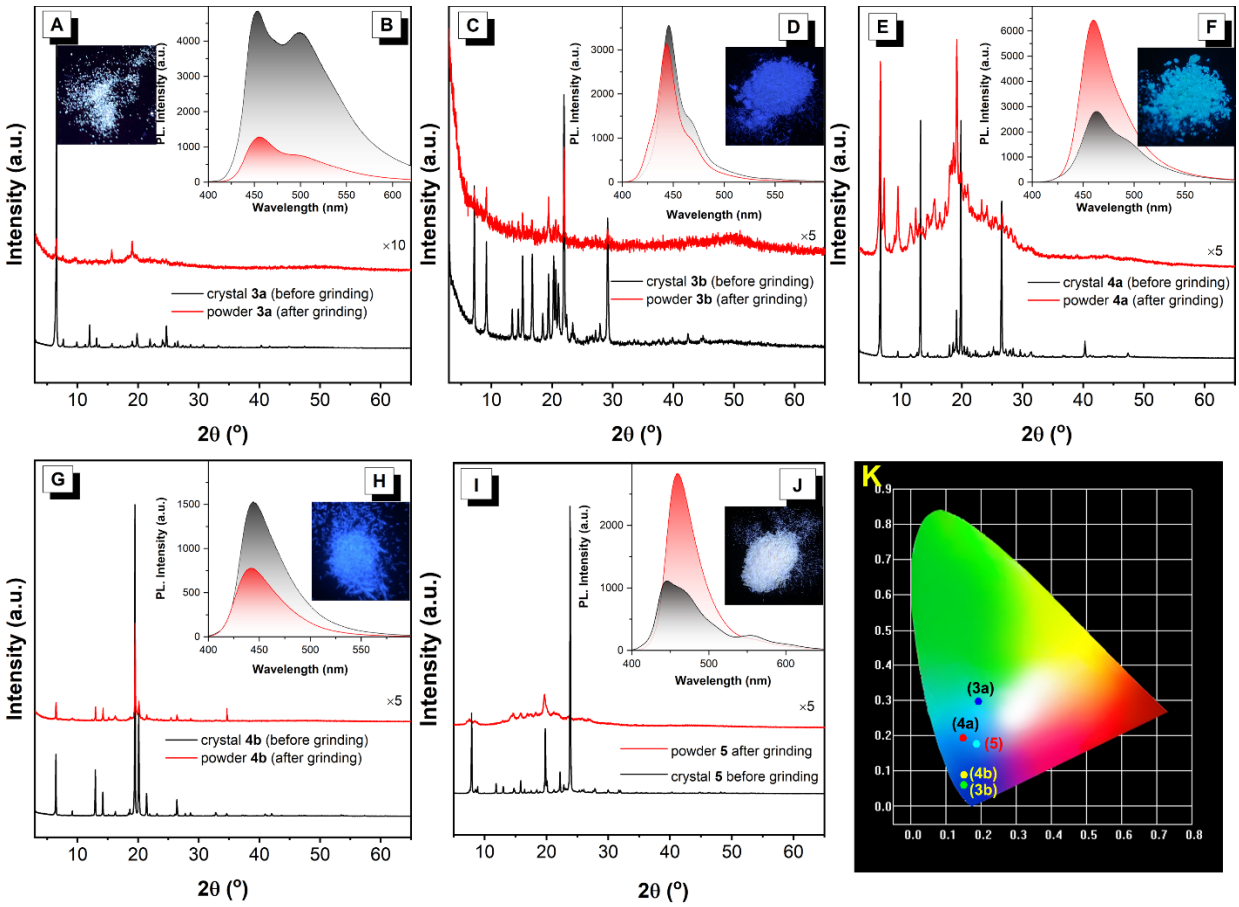

Figure 5. Wide angle XRD diffractograms of compounds (A) **3a**, (C) **3b**, (E) **4a**, (G) **4b** and (I) **5** in the crystal state and in the grinding state, respectively. The PL spectra of (B) **3a**, (D) **3b**, (F) **4a**, (H) **4b** and (J) **5** in the crystal state and in the grinding state, (K) CIE coordinates of the crystal **3-5** in the crystal state. Insert: the photograph of the corresponding compounds **3-5** in the crystal state under UV irradiation (λ_{ex} = 365 nm).

On the other hand, compared to their crystal state, upon applying external force, the emission intensity of **3a**, **3b** and **4b** decreased upon grinding with decreased fluorescent quantum yields (Φ_f) of 0.02, 0.04 and 0.12, respectively. However, the emission intensity of compounds **4a** is enhanced with an increased Φ_f of 0.11. Interestingly, the ground compound **5** emits blue emission with the maximum λ_{em} at 458 nm with Φ_f of 0.86, while the excimer emission at 555 nm almost disappeared, implying that the ground-state dimers tend to form monomers under external stimuli. In addition, the compound **4b** exhibits a narrower FWHM (23 nm) in the powder compared to 1,3,6,8- tetrakis(4-trifluorophenyl)-pyrene (Figure S41 and Table S6).[36,39] Moreover, the CIEy of compounds **3-5** become smaller indicating that these compounds tend to be pure blue emitters after grinding (Figure S42 and Table S7).

To understand the relationship between the optical properties and the crystal patterns of this new pyrene family, X-ray powder diffraction was performed to investigate the changes of the molecular packing before and after grinding. As shown in Figure 5, the crystals **3-5** exhibit clear and intense XRD patterns, which are consistent with the simulated XRD powder patterns obtained from their single crystal X-ray structures, and indicate that all of compounds are highly crystalline without other potential polymorphs.[45]

Moreover, according to their XRD patterns, the diffract peak at 2θ = 6.554° for **3a**, at 7.172° for **3b**, at 6.558 ° for **4a** and at 7.871° for **5** fit well with the (200) diffraction peaks based on their single-crystal X-ray diffraction data, and the calculated d-spacing between the layers are 13.4753 Å, 12.3149 Å and 13.4671 Å and 11.2237 Å, respectively, which is close to half the value of the *a*-axis of their unit cells. The diffraction peak of **4b** at 6.434° is consistent with the (001) phase (*c*-axis), and the corresponding d-spacing is 13.7270 Å. After grinding, although the intensity of the diffraction peaks rapidly decreased, we found that the space group of the grinding samples remained the same as for the corresponding crystalline samples (Table S5) according to the curve fit from the XRD. Thus, the grinding samples **3-5** are still in the microcrystalline state with reduced crystal size according to the Scherrer equation ($D = k\lambda/\cos\theta$).[46] Compared with the XRD pattern of the crystal (before grinding), after grinding sample, the d-spacing values of **3a**, **3b** and **4a** between layers along the *a*-axis direction (and **4b** along c-axis) increases to 13.5915 Å, 12.3422 Å, 13.5418 Å, 13.6562 Å and 11.6924 Å, respectively, indicating that the crystals prefer to shift along the (200) (and **4b** along (001)) lattice plane upon applying a mechanical stimulation.

Combining the results of the crystal packing, the simulated PXRD patterns from the crystals and the experimental XRD patterns, the diffraction peaks of the crystal in the region of 2θ = 18 ° -20 ° corresponds with weak intermolecular interactions between the pyrene molecules. The PXRD peak in the region 2θ = 20 ° -25 ° is tentatively assigned to a π-π stacking interaction. For example, after grinding, although the XRD diffraction peaks of **3b** at 2θ = 7.172 ° and 29.132 ° are absent, the main diffraction peak at 2θ = 21.967 ° is still present with a decreased d-spacing from 4.0465 Å to 4.043 Å (2θ = 21.947 °), which is consistent with the face-to-face π-π stacking interaction. This indicates that the π-π stacking interaction becomes more dominant, which is in good agreement with their crystal packing. When grinding the crystal **3b**, the molecule becomes more planar and

strengthens the π···π stacking interactions. Similarly, according to the PXRD pattern, the average distance between the molecules decreases compared to the crystals via the strength of the C-H···π interactions in **3a** and **4b**. Thus, crystals **3a**, **3b** and **4b** show a decreased emission intensity after grinding.

By contrast, when grinding the crystal **4a**, the diffraction peak at 2θ = 6.558 º was divided into two peaks at 2θ = 6.522 º and 7.173 º with an increased d-spacing along the (200) phase, and the primary peak at 2θ = 19.810 º was shifted to 19.143 º, and the d-spacing value increased from 4.4779 Å to 4.6326 Å. This indicates that the intermolecular interactions (such as C-H···π interaction) between molecules became weaker after grinding. Similarly, the main diffraction peaks of the crystal **5** are located at 2θ = 19.795 º and 23.809 º, with the d-spacing value of 4.4813 Å and 3.7341 Å, respectively. Although both the intensity of these peaks (2θ = 19.690 º and 23.803 º) decreased after grinding, the d-spacing values still increased, meaning that the molecular packing patterns became loose, and the loose packing mode in **4a** and **5** is beneficial for enhancing the radiative transition and results in improved fluorescence emission and quantum yield.

To understand the intermolecular interactions in the molecular arrangement and emission behavior, the Hirshfeld surfaces and two-dimensional (2D) fingerprint was used for the quantified analysis of the types of intermolecular interaction present in their crystal structures. The red, green and blue areas on the surfaces indicate the strength of the intermolecular interaction, which follow the order red areas > green areas > blue areas. As shown in Figure 6, and Table S11-S12, the weak interactions, such as C-H···π and C-O···H play a dominant role in the crystals **3a**, **4a** and **5**, and are indicated by the red areas via the Hirshfeld surfaces analysis. Also, other non-covalent interactions are observed. On the other hand, for the compounds **3b** and **4b** containing trifluoromethyl units, the contribution of C-F···H and C-H···π can be identified on the Hirshfeld

surface with red areas, and the C-F···H interactions are over 28.7% and 40.2% of the total Hirshfeld surfaces in **3b** and **4b**, respectively. Obviously, the C-F···H interactions are stronger than the C-H···π interactions (16.5% for **3b** and 18.1% in **4b**) in the respective crystals.

Thus, according to the Hirshfeld surface analysis, the presence of a number of C-H···π and the C-O···H interactions can induce charge-transfer emission/ excimer emission in the solid state, leading to dual emission in crystals **3a** and **5**. Meanwhile, the synergetic effect of the stronger C-F···H interaction and the C-H···π interaction in crystals **3b** and **4b** can contribute to a decrease of the quantum yield in the crystal state. This conclusion is in good agreement with our spectroscopic results.

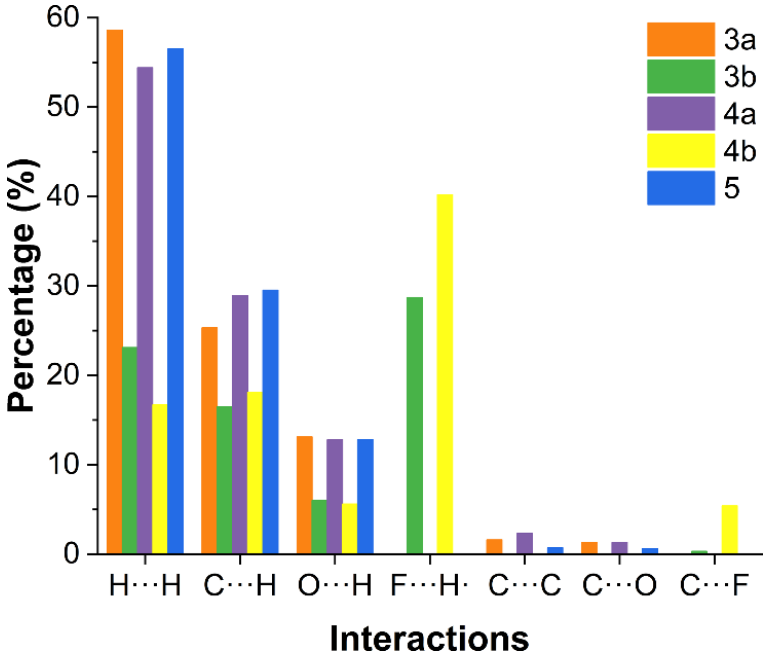

Figure 6. Histogram representing various intermolecular interactions in crystals **3**, **4** and **5**.

4. Conclusions

This article presents two novel bromopyrene intermediates, namely, 1,3,6,8-tetraaryl,2-hydroxypyrenes and 1,3,6,8-tetraaryl 2,7-dihydroxypyrenes which are utilized to prepare novel

pyrene-based luminescent materials, via a Suzuki-Miyaura cross-coupling reaction. The star-shaped pyrene derivatives containing an -OH group at the 2- or 2,7-positions possess favorable optical properties, such as narrow FWHM blue emission both in solution and in the solid state. Also, due to the presence of the -OH group at the 2- or 2,7-positions, the intermolecular interactions between pyrenes are strengthened via H-bond interactions, leading to an extremely low fluorescence quantum yield in the crystal state. The -OH group at the 2-position of pyrene still displays a high reactivity, and can be further involved in a methylation reaction to afford a blue emitter **5**, which also displays a dual emission with mechanical force-induced enhanced emission with a high quantum yield in the solid state. The presence of H-bonds plays an important role to regulate the intermolecular interactions (such as C-H···π, the C-O···H and π-π stacking etc.), leading to exciting emission behavior. This present study not only provides new bromopyrene intermediates for constructing the next-generation of pyrene-based emitters for potential applications as organic electronics via the functionalization of the pyrene both at the 1,3,6,8- and 2,7-positions, but also opens up a potential pathway for the exploitation of blue materials with mechanical force-induced enhanced emission properties. Further experimental and theoretical calculations are on-going in our laboratory.

2. Experimental

2.1 Materials

Unless otherwise stated, all reagents used were purchased from commercial sources and were used without further purification. Tetrahydrofuran was distilled prior to use.

2.2 Characterization

^{1}H and ^{13}C NMR spectra were recorded on a Bruker AV 400M spectrometer using chloroform-*d* solvent and tetramethylsilane as internal reference. *J*-values are given in Hz. High-resolution mass

spectra (HRMS) were recorded on a LC/MS/MS, which consisted of a HPLC system (Ultimate 3000 RSLC, Thermo Scientific, USA) and a Q Exactive Orbitrap (QE orbitrap type) mass spectrometer. UV-vis absorption spectra and photoluminescence (PL) spectra were recorded on a Shimadzu UV-2600 and the Hitachi F-4700 spectrofluorometer. PL quantum yields were measured using absolute methods using a Hamamatsu C11347-11 Quantaurus-QY Analyzer. The lifetime was recorded on an Edinburgh FLS 980 instrument and measured using a time-correlated single-photon counting method. Thermogravimetric analysis was carried on a Mettler Toledo TGA/DSC3+ under dry nitrogen at a heating rate of 10 ^{o}C/min. The quantum chemistry calculation was performed on the Gaussian 09 (B3LYP/6–311G (d,p) basis set) software package.

2.3 X-ray Crystallography

Crystallographic data for the compounds was collected on a Bruker APEX 2 CCD diffractometer with graphite monochromated Mo Kα radiation (λ = 0.71073 Å) in the ω scan mode. [47, 48] The structures were solved by charge flipping or direct methods algorithms and refined by full-matrix least-squares methods on F^2.[49] All esds (except the esd in the dihedral angle between two l.s. planes) were estimated using the full covariance matrix. The cell esds were considered individually in the estimation of esds in distances, angles and torsion angles. Correlations between esds in cell parameters were only used when they were defined by crystal symmetry. An approximate (isotropic) treatment of cell esds was used for estimating esds involving l.s. planes. The final cell constants were determined through global refinement of the xyz centroids of the reflections harvested from the entire data set. Structure solution and refinements were carried out using the SHELXTL-PLUS software package.[49] The partially occupied water molecule of crystallization was modelled by the Platon Squeeze procedure. Data (excluding structure factors) on the structures reported here have been deposited with the Cambridge Crystallographic Data Centre. CCDC

2128127 (**3a**), 2128128 (**3b**), 2128129 (**4b**), 2128130 (**4a**), 2128131 (**5**) contains the supplementary crystallographic data for this paper. These data could be obtained free of charge from The Cambridge Crystallographic Data Centre via www.ccdc.cam.ac.uk/data_request/cif.

2.4 Synthetic procedures

Synthesis of 2,7-dihydroxypyrene (Py-2OH).[32]

Under a nitrogen atmosphere, pyrene-2,7-bis(4,4,5,5-tetramethyl-[1,3,2]dioxaborolane) (908 mg, 2.0 mmol, 1.0 eq.) and NaOH (480 mg, 12 mmol, 6 eq.) were dissolved in 60 mL THF, and the mixture was stirred for 10 minutes, then H_2O_2 (1.5 ml, 30%) and 3 ml H_2O was added into the reaction bottle. After stirring for 6 h at room temperature, the solution was acidified to pH 1–2 by using 1 M HCl. Then, the product was evaporated and extracted with ethyl acetate (3 × 30 ml) three times, washed with saturated brine (50 mL), and dried with $MgSO_4$. The organic phase was evaporated and the residue was dissolved in 3 ml ethyl acetate, then, the solvent ethanol (200 mL) was added until the precipitate appears, which was further filtered under reduced pressure to afford compound **Py-2OH** as a brown powder (446 mg, 95% yield). ^{1}H NMR (400 MHz, [D6]-DMSO) δ 9.88 (s, 2H), 7.94 (s, 4H), 7.60 (s, 4H) ppm, which is consistent with Marder's report.[32]

Synthesis of 2-hydroxypyrene (Py-OH).[34]

Under a nitrogen atmosphere, pyrene-2-(4,4,5,5-tetramethyl-[1, 3, 2]dioxaborolane) [50] (600 mg, 1.8 mmol, 1.0 eq.) and NaOH (270 mg, 4.6 mmol, 2.5 eq.) were dissolved in THF (70 mL), and the mixture was stirred for 10 minutes. To this mixture, an aqueous solution of H_2O_2 (0.5 mL, 30%) and 1 mL H_2O was added into the reaction bottle. After stirring for 4 h at room temperature, the solution was acidified to pH 1–2 by using 1 M HCl. Then, the product was evaporated and extracted with dichloromethane (3 × 30 mL) three times, washed with saturated brine (50 mL), and dried with $MgSO_4$. The organic phase was evaporated and the residue was dissolved in 3 mL

ethyl acetate, then, the solvent ethanol (200 mL) was added until the precipitate appears, which was further filtered under reduced pressure to afford compound **Py-OH** as a bright-brown solid (360 mg, 91% yield). ^{1}H NMR (400 MHz, d-$CDCl_3$, TMS): δ 8.16 (d, J = 7.6 Hz, 2H), 8.06 (d, J = 9.0 Hz, 2H), 7.98-7.90 (m, 3H), 7.64 (s, 2H), 5.45 (s, 1H, OH) ppm, which is consistent with Marder's report.[34]

Synthesis of 1,3,6,8-tetrabromo-2,7-dihydroxy pyrene (1)

Under a nitrogen atmosphere, a mixture of bromine (1.4 mL, 25.6 mmol, 8 eq.) with 10 mL nitrobenzene was added dropwise to a solution of **Py-2OH** (750 mg, 3.2 mmol, 1 eq.) in nitrobenzene (40 mL). The mixture was vigorously stirred at 120 ºC for 24 h. After cooling to room temperature to yield a brown precipitate, the mixture was filtered with hexane (200 mL) under reduced pressure to afford compound **1** as a light-green solid (1.61 g, yield at 91%), which was insoluble in common organic solvents, such as chloroform and DMSO, but slightly dissolve in ethanol. The product was not further purified and was used as such for the Suzuki coupling reactions directly. The solid was characterized by HRMS. HRMS (FTMS + p APCI) m/z: found, 548.6986 $[M-H]^+$; calcd for $C_{16}H_6Br_4O_2$ requires $[M]^+$ 549.8336.

Synthesis of 1,3,6,8-tetrabromo-2-hydroxypyrene (2)

The compound **2** was synthesized by the same procedure as for **1**. The compound **2** is a bright-brown solid (1.82 g, yield at 92%), which was insoluble in common organic solvents, such as chloroform and DMSO, but slightly dissolved in ethanol. The product was not further purified and was used as such for the Suzuki coupling reactions directly. The solid was characterized by HRMS. HRMS (FTMS - p APCI) m/z: found, 532.7036 $[M-H]^+$; calcd for $C_{16}H_6Br_4O$ requires $[M]^+$ 533.8342.

Synthesis of 1,3,6,8-tetrakis(*4-methoxyphenyl*)-2,7-dihydroxypyrene (3a)

Under a nitrogen atmosphere, a mixture of **1** (110 mg, 0.2 mmol, 1.0 eq.), 4-methoxyphenyl boronic acid (183 mg, 1.2 mmol, 6 eq.) and K_2CO_3 (500 mg, 3.6 mmol, 18 eq.) were dissolved in tetrahydrofuran (8 mL) and stirred for 5 min. Then, $Pd(PPh_3)_4$ (50 mg, 0.04 mmol, 0.2 eq.) was added. The mixture was vigorously stirred at 90℃ for 24 h. After cooling to room temperature, the reaction mixture was quenched with water (50 mL) and extracted with CH_2Cl_2 three times (3 × 30 mL). The combined organic layer was washed with water and brine (100 mL), dried over $MgSO_4$ and evaporated. The crude product was further purified by column chromatography with hexane/dichloromethane (V_{hexane}: V_{CH2Cl2} = 2:1) as the eluent to afford 1,3,6,8-tetrakis(*4-methoxyphenyl*)-2,7-dihydroxypyrene (**3a**) as a yellow solid, which was recrystallization from $CHCl_3$/hexane to afford **3a** as a yellow solid (62 mg, 47%, melting point > 300 ^oC). ^1H NMR (400 MHz, $CDCl_3$) δ 7.69 (s, 4H), 7.47 (d, *J* = 8.6 Hz, 8H), 7.11 (d, *J* = 8.6 Hz, 8H), 5.37 (s, 2H), 3.91 (s, 12H) ppm. ^{13}C {^1H} NMR (101 MHz, $CDCl_3$) δ 159.4, 132.5, 129.4, 127.5, 125.3, 123.5, 120.2, 114.5, 55.4 ppm. HRMS (FTMS + p APCI) m/z: found, 659.2410 $[M+H]^+$; calcd for $C_{44}H_{34}O_6$ requires $[M+H]^+$ 659.2389.

Synthesis of 1,3,6,8-tetrakis(4-trifluorophenyl)-2,7-di hydroxypyrene (3b)

Under a nitrogen atmosphere, **1** (220 mg, 0.4 mmol, 1.0 eq.), 4-(trifluoromethyl)phenylboronic acid (456 mg, 2.4 mmol, 6 eq.) and K_2CO_3 (1 g, 7.2 mmol, 18 eq.) were dissolved in a mixture of THF (8 mL)/ H_2O (2 mL) and stirred for 5 min. Then, $Pd_2(dba)_3$ (29.3 mg, 0.032 mmol, 0.08 eq.) and $(t\text{-}Bu)_3PBF_4$ (26.8 mg, 0.128 mmol, 0.32 eq.) were added, and the mixture was vigorously stirred at 90℃ for 24 h. After cooling to room temperature, the reaction mixture was quenched with water (50 mL) and extracted with ethyl acetate three times (3 × 30 mL). The combined organic layer was washed with water and brine (100 mL), dried over $MgSO_4$ and evaporated. The crude product was purified by column chromatography with hexane/ ethyl acetate (V_{hexane}: $V_{ethyl\ acetate}$

= 10:1) as the eluent and recrystallized in a mixture of $CHCl_3$ and hexane to yield 1,3,6,8-tetrakis(4-trifluorophenyl)-2,7-dihydroxypyrene (**3b**) as a transparent solid (124 mg, 38%). ^{1}H NMR (400 MHz, $CDCl_3$) δ 7.86 (d, *J* = 8.0 Hz, 8H), 7.70 (d, *J* = 7.9 Hz, 8H), 7.64 (s, 4H), 5.14 (s, 2H) ppm. ^{13}C NMR (101 MHz, $CDCl_3$) δ 147.2, 139.0, 131.8, 130.8, 130.5, 129.4, 126.1, 126.0, 125.6, 123.0, 120.0 ppm. HRMS (FTMS - p APCI) m/z: found, 809.1394 $[M-H]^+$; calcd for $C_{44}H_{22}F_{12}O_2$ requires $[M-H]^+$ 809.1355.

Synthesis of 1,3,6,8-tetrakis(*4-methoxyphenyl*)-2-hydroxy pyrene (4a)

Under a nitrogen atmosphere, **2** (110 mg, 0.2 mmol, 1.0 eq.), 4-methoxyphenyl boronic acid (183 mg, 1.2 mmol, 6 eq.) and K_2CO_3 (500 mg, 3.6 mmol, 18 eq.) were dissolved in a mixture of toluene (10 mL)/ ethanol (2 mL)/ H_2O (2 mL) and stirred for 5 min. Then, $Pd(PPh_3)_4$ (50 mg, 0.04 mmol, 0.2 eq.) was added, and the mixture was vigorously stirred at 90℃ for 24 h. After cooling to room temperature, the reaction mixture was washed with water (150 mL) and extracted with CH_2Cl_2 three times (3 × 30 mL). The combined organic layer was washed with water and brine (100 mL), dried over $MgSO_4$ and evaporated. The crude product was purified by column chromatography with hexane/dichloromethane (V_{hexane}: V_{CH2Cl2} = 2:1) as the eluent to afford **4a** as a yellow solid (90 mg, 70%, melting point > 300 ºC). ^{1}H NMR (400 MHz, $CDCl_3$) δ 8.10 (d, *J* = 9.5 Hz, 2H), 7.88 (s, 1H), 7.75 (d, *J* = 9.5 Hz, 2H), 7.57 (d, *J* = 8.6 Hz, 4H), 7.50 (d, *J* = 8.6 Hz, 4H), 7.13 (d, *J* = 8.7 Hz, 4H), 7.06 (d, *J* = 8.7 Hz, 4H), 5.45 (s, 1H), 3.92 (s, 6H), 3.91 (s, 6H) ppm. ^{13}C {^{1}H} NMR (101 MHz, $CDCl_3$) δ 159.4, 159.0, 148.7, 137.3, 133.6, 132.6, 131.7, 130.6, 128.7, 127.5, 126.9, 125.8, 125.7, 124.7, 122.9, 120.7, 114.5, 113.8, 55.4, 55.4, 53.5 ppm. HRMS (FTMS + p APCI) m/z: found, 643.2477 $[M+H]^+$; calcd for $C_{44}H_{34}O_5$ requires $[M+1]^+$ 643.2440.

Synthesis of 1,3,6,8-tetrakis(4-trifluorophenyl)- 2-hydroxypyrene (4b)

Under a nitrogen atmosphere, **2** (83 mg, 0.16 mmol, 1.0 eq.), 4-(trifluoromethyl)phenylboronic acid (177 mg, 0.93 mmol, 6 eq.) and K_2CO_3 (500 mg, 3.6 mmol, 22.5 eq.) were dissolved in a mixture of THF (8 mL)/ H_2O (2 mL) and stirred for 5 min. Then, $Pd_2(dba)_3$ (12 mg, 1.3 mmol, 0.08 eq.) and $(t\text{-Bu})_3PBF_4$ (11 mg, 5.12 mmol, 0.32 eq.) were added, and the mixture was vigorously stirred at 90℃ for 24 h. After cooling to room temperature, the reaction mixture was quenched with water (50 mL) and extracted with CH_2Cl_2 three times (3 × 30 mL). The combined organic layer was washed with water and brine (100 mL), dried over $MgSO_4$ and evaporated. The crude product was purified by column chromatography with hexane/dichloromethane (V_{hexane}: V_{CH2Cl2} = 3:1) as the eluent and recrystallized in a mixture of $CHCl_3$ and hexane to yield **4b** as a white solid (78 mg, 65%, melting point > 300 ºC). ^{1}H NMR (400 MHz, DMSO-d6) δδ 8.31 (s, 1H), 8.04 (d, *J* = 9.6 Hz, 2H), 7.99 – 7.88 (m, 13H), 7.75 (d, *J* = 7.9 Hz, 4H), 7.66 (d, *J* = 9.6 Hz, 2H) ppm. ^{13}C {^{1}H} NMR (101 MHz, $CDCl_3$) δ 148.0, 144.2, 139.0, 136.7, 131.9, 130.9, 130.6, 130.5, 130.0, 129.7, 128.3, 127.3, 126.1, 126.1, 126.0, 125.6, 125.4, 125.4, 125.4, 125.2, 122.9, 122.8, 122.7, 120.4 ppm. HRMS (FTMS - p APCI) m/z: found, 793.1407 $[M\text{-}H]^+$; calcd for $C_{44}H_{22}F_{12}O$ requires $[M\text{-}H]^+$ 793.1401.

Synthesis of 1,3,6,8-tetrakis(*4-methoxyphenyl*)-2- methoxylpyrene (5)

Under a nitrogen atmosphere, a mixture of **4a** (130 mg, 0.20 mmol, 1 eq.), iodomethane (8.1 mmol, 500 uL), and K_2CO_3 (240 mg, 1.7 mmol, 16 eq.) in acetonitrile (5 mL) was heated under reflux overnight. TLC analysis indicated the formation of new spots. After cooling, H_2O was added to the residue and the mixture was extracted with CH_2Cl_2 three times, washed with brine, and dried with anhydrous Mg_2SO_4 and evaporated under reduced pressure. The residue was purified by column chromatography (silica, V_{hexane}: V_{CH2Cl2} = 4:1) to afford the product as a white solid (82 mg, 70%, melting point > 300 ºC.). ^{1}H NMR (400 MHz, $CDCl_3$) δ 8.11 (d, *J* = 9.6 Hz, 2H), 7.92

(s, 1H), 7.86 (d, *J* = 9.6 Hz, 2H), 7.57 (d, *J* = 8.7 Hz, 4H), 7.51 (d, *J* = 8.7 Hz, 4H), 7.12 – 7.03 (m, 8H), 3.92 (s, 6H), 3.91 (s, 6H) ppm, 3.22 (s, 3H). ^{13}C {^{1}H}c NMR (101 MHz, $CDCl_3$) δ 159.0, 158.9, 157.2, 137.1, 133.5, 132.4, 131.7, 131.6, 130.8, 130.5, 129.2, 129.1, 127.5, 127.4, 125.5, 125.2, 120.1, 113.8, 113.6, 110.7, 60.8, 55.8, 55.4, 55.4 ppm. HRMS (FTMS + p APCI) m/z: found, 657.2621 $[M+H]^+$; calcd for $C_{45}H_{36}O_5$ requires $[M+H]^+$ 657.2596.

ASSOCIATED CONTENT

Supporting Information

The Supporting Information is available free of charge on the ACS Publications website.

Additional experimental methods for the pyrene-based derivatives. Details of the experimental characterization, including $^{1}H/^{13}C$ NMR spectra, HRMS, Results of UV−vis and fluorescence spectra, crystal parameters, TD-DFT calculations (PDF) and Hirshfeld Surfaces Analysis.

Single crystal X-ray diffraction of **3-5** (CIF)

NMR FID files for compounds **3-5** (ZIP)

AUTHOR INFORMATION

Corresponding Author

Xing Feng-Guangdong Provincial Key Laboratory of Information Photonics Technology, School of Material and Energy, Guangdong University of Technology, Guangzhou 510006, P. R. China, E-mail: hyxhn@sina.com.

Ben Zhong Tang - Shenzhen Institute of Aggregate Science and Technology, School of Science and Engineering, The Chinese University of Hong Kong, Shenzhen 518172, China; AIE Institute, Guangzhou 510530, China. Email: tangbenz@cuhk.edu.cn

Author Contributions

Xiaohui Wang - Guangdong Provincial Key Laboratory of Information Photonics Technology, School of Material and Energy, Guangdong University of Technology, Guangzhou 510006, P. R. China. ORCID: 0000-0001-7506-2845

Jianyu Zhang- Department of Chemistry, The Hong Kong Branch of Chinese National Engineering Research Center for Tissue Restoration and Reconstruction, Institute for Advanced Study and Department of Chemical and Biological Engineering, The Hong Kong University of Science and Technology, Clear Water Bay, Kowloon, Hong Kong, China.

Xiaoyu Mao - Guangdong Provincial Key Laboratory of Functional Soft Condensed Matter, School of Material and Energy, Guangdong University of Technology, Guangzhou 510006, P. R. China

Yiwei Liu - Guangdong Provincial Key Laboratory of Functional Soft Condensed Matter, School of Material and Energy, Guangdong University of Technology, Guangzhou 510006, P. R. China

Ruikuan Li- Guangdong Provincial Key Laboratory of Functional Soft Condensed Matter, School of Material and Energy, Guangdong University of Technology, Guangzhou 510006, P. R. China

Jie Bai- Guangdong Provincial Key Laboratory of Functional Soft Condensed Matter, School of Material and Energy, Guangdong University of Technology, Guangzhou 510006, P. R. China

Jun Zhang- School of Materials and Chemical Engineering, Anhui Jianzhu University, Hefei, 230601, P. R. China.

Carl Redshaw- Department of Chemistry, University of Hull, Cottingham Road, Hull, Yorkshire HU6 7RX, UK.

Notes

The authors declare no competing financial interest.

ACKNOWLEDGMENT

This work was supported by the National Natural Science Foundation of China (21975054), Natural Science Foundation of Guangdong Province of China (2019A1515010925), Guangdong Provincial Key Laboratory of Information Photonics Technology (2020B121201011), “One Hundred Talents Program” of the Guangdong University of Technology (GDUT) (1108-220413205), the Open Fund of Guangdong Provincial Key Laboratory of Luminescence from Molecular Aggregates, Guangzhou 510640, China (South China University of Technology) (2019B030301003), Science and Technology Planning Project of Hunan Province (2018TP1017), CR thanks the EPSRC for an Overseas Travel Grant (EP/R023816/1).

References

(1) Kim, S. G.; Kim, K. H.; Kim, Y. K.; Shin, S. K.; Ahn, K. H. Crucial role of three-center hydrogen bonding in a challenging chiral molecular recognition. *J. Am. Chem. Soc.* **2003**, *125*, 13819-13824, DOI: 10.1021/ja037031p.

(2) Xu, W.; Arieno, M.; Low, H.; Huang, K.; Xie, X.; Cruchter, T.; Ma, Q.; Xi, J.; Huang, B.; Wiest, O.; Gong, L.; Meggers, E. Metal-Templated Design: Enantioselective Hydrogen-Bond-Driven Catalysis Requiring Only Parts-per-Million Catalyst Loading. *J. Am. Chem. Soc.* **2016**, *138*, 8774-8780, DOI: 10.1021/jacs.6b02769.

(3) Clegg, J. K.; Siddique, R. G.; Arachchige, K. S. A.; Fayaad, H. A. A. L.; Thoburn, J. D.; McMurtrie, J. C. Controlling the Complexity and Interconversion Mechanisms in Self‐assembled [Fe2L3]4+ Helicates and [Fe4L6]8+ Coordination Cages. *Angew. Chem. Int. Ed.* **2021**, DOI: 10.1002/anie.202115555.

(4) Jiang, N.; Ruan, S. H.; Liu, X. M.; Zhu, D.; Li, B.; Bryce, M. R. Supramolecular Oligourethane Gel with Multicolor Luminescence Controlled by Mechanically Sensitive Hydrogen-Bonding. *Chem. Mater.* **2020,** *32* (13), 5776-5784, DOI: 10.1021/acs.chemmater.0c01620.

(5) Vazquez-Gonzalez, M.; Willner, I. Stimuli-Responsive Biomolecule-Based Hydrogels and Their Applications. *Angew. Chem. In.t Ed.* **2020,** *59* (36), 15342-15377, DOI: 10.1002/anie.201907670.

(6) Laurent, A. *Ann. Chim. Phys.* **1837**, *66*, 136.

(7) Figueira-Duarte, T. M.; Mullen, K. Pyrene-based materials for organic electronics. *Chem. Rev.* **2011,** *111* (11), 7260-314, DOI: 10.1021/cr100428a.

(8) Li, D.; Song, J.; Yin, P.; Simotwo, S.; Bassler, A. J.; Aung, Y.; Roberts, J. E.; Hardcastle, K. I.; Hill, C. L.; Liu, T. Inorganic-organic hybrid vesicles with counterion- and pH-controlled fluorescent properties. *J. Am. Chem. Soc.* **2011,** *133* (35), 14010-14016, DOI: 10.1021/ja204034g.

(9) Ayyavoo, K.; Velusamy, P. Pyrene based materials as fluorescent probes in chemical and biological fields. *New J. Chem.* **2021,** *45* (25), 10997-11017, DOI: 10.1039/d1nj00158b.

(10) Islam, M. M.; Hu, Z.; Wang, Q.; Redshaw, C.; Feng, X. Pyrene-based aggregation-induced emission luminogens and their applications. *Mater. Chem. Front.* **2019,** *3* (5), 762-781, DOI: 10.1039/c9qm00090a.

(11) Liang, Y.; Jing, Y.; Gheytani, S.; Lee, K. Y.; Liu, P.; Facchetti, A.; Yao, Y. Universal quinone electrodes for long cycle life aqueous rechargeable batteries. *Nat. Mater.* **2017,** *16* (8), 841-848, DOI: 10.1038/nmat4919.

(12) Kinik, F. P.; Ortega-Guerrero, A.; Ongari, D.; Ireland, C. P.; Smit, B. Pyrene-based metal organic frameworks: from synthesis to applications. *Chem. Soc. Rev.* **2021,** *50* (5), 3143-3177, DOI: 10.1039/d0cs00424c.

(13) Anetai, H.; Wada, Y.; Takeda, T.; Hoshino, N.; Yamamoto, S.; Mitsuishi, M.; Takenobu, T.; Akutagawa, T. Fluorescent Ferroelectrics of Hydrogen-Bonded Pyrene Derivatives. *J. Phys. Chem. Lett.* **2015,** *6* (10), 1813-1818, DOI: 10.1021/acs.jpclett.5b00703.

(14) Sagara, Y.; Mutai, T.; Yoshikawa, I.; Araki, K. Material design for piezochromic luminescence: hydrogen-bond-directed assemblies of a pyrene derivative. *J. Am. Chem. Soc.* **2007,** *129* (6), 1520-1, DOI: 10.1021/ja0677362.

(15) Feng, X.; Hu, J. Y.; Redshaw, C.; Yamato, T. Functionalization of Pyrene To Prepare Luminescent Materials-Typical Examples of Synthetic Methodology. *Chem. Eur. J.* **2016,** *22* (34), 11898-916, DOI: 10.1002/chem.201600465.

(16) Feng, X. D., Yanping; Wei, Xianfu; Yamato, Takehiko *Pyrene-Based Advanced Luminescence Materials-Synthesis, Structure and Application*; Chinese Science & Technic Press, 2016.

(17) Allen, A. D.; Tidwell, T. T. Ketenes and other cumulenes as reactive intermediates. *Chem. Rev.* **2013,** *113* (9), 7287-342, DOI: 10.1021/cr3005263.

(18) Hu, J.; Zhang, D.; Harris, F. W. Ruthenium(III) chloride catalyzed oxidation of pyrene and 2,7-disubstitued pyrenes: an efficient, one-step synthesis of pyrene-4,5-diones and pyrene-4,5,9,10-tetraones. *J. Org. Chem.* **2005**, *70*, 707-708. DOI: 10.1021/jo048509q

(19) Kulisic, N.; More, S.; Mateo-Alonso, A. A tetraalkylated pyrene building block for the synthesis of pyrene-fused azaacenes with enhanced solubility. *Chem. Commun.* **2011**, *47*, 514-516. DOI: 10.1039/C0CC02249G

(20) El-Assaad, T. H.; Parida, K. N.; Cesario, M. F.; McGrath, D. V. Sterically driven metal-free oxidation of 2,7-di-tert-butylpyrene. *Green Chem.* **2020**, *22*, 5966- 5971. DOI: 10.1039/D0GC02000A

(21) More, S.; Bhosale, R.; Choudhary, S.; Mateo-Alonso, A. Versatile 2,7-substituted pyrene synthons for the synthesis of pyrene-fused azaacenes. *Org. Lett.* **2012**, *14*, 4170- 4173. DOI: 10.1021/ol301841h

(22) Mateos-Martin, J.; Carini, M.; Melle-Franco, M.; Mateo-Alonso, A. Increasing and dispersing strain in pyrene-fused azaacenes. *Chem. Commun.* **2020**, *56*, 11457-11460. DOI: 10.1039/D0CC04735J

(23) Bhosale, S. V.; Al Kobaisi, M.; Jadhav, R. W.; Morajkar, P. P.; Jones, L. A.; George, S. Naphthalene diimides: perspectives and promise. *Chem. Soc. Rev.* **2021,** *50* (17), 9845-9998, DOI: 10.1039/d0cs00239a.

(24) Feng, X.; Qi, C.; Feng, H. T.; Zhao, Z.; Sung, H. H. Y.; Williams, I. D.; Kwok, R. T. K.; Lam, J. W. Y.; Qin, A.; Tang, B. Z. Dual fluorescence of tetraphenylethylene-substituted pyrenes with aggregation-induced emission characteristics for white-light emission. *Chem. Sci.* **2018,** *9* (25), 5679-5687, DOI: 10.1039/c8sc01709c.

(25) Wang, X. H.; Wang, L. R.; Mao, X. Y.; Wang, Q. S.; Mu, Z. F.; An, L.; Zhang, W.; Feng, X.; Redshaw, C.; Cao, C. Y.; Qin, A. J.; Tang, B. Z. Pyrene-based aggregation-induced emission luminogens (AIEgens) with less colour migration for anti-counterfeiting applications. *J. Mater. Chem. C* **2021,** *9* (37), 12828-12838, DOI: 10.1039/d1tc03022a.

(26) Feng, X.; Xu, Z.; Hu, Z.; Qi, C.; Luo, D.; Zhao, X.; Mu, Z.; Redshaw, C.; Lam, J. W. Y.; Ma, D.; Tang, B. Z. Pyrene-based blue emitters with aggregation-induced emission features for

high-performance organic light-emitting diodes. *J. Mater. Chem. C* **2019,** *7* (8), 2283-2290, DOI: 10.1039/c8tc05547e.

(27) Vollmann, H.; Becker, H.; Corell, M.; Streeck, H. Beiträge zur Kenntnis des Pyrens und seiner Derivate. *Justus Liebig's Annalen der Chemie* **1937,** *531* (1), 1-159, DOI: 10.1002/jlac.19375310102.

(28) Hu, J.-Y.; Era, M.; Elsegood, M. R. J.; Yamato, T. Synthesis and Photophysical Properties of Pyrene-Based Light-Emitting Monomers: Highly Pure-Blue-Fluorescent, Cruciform-Shaped Architectures. *Eur. J. Org. Chem.* **2010,** *2010* (1), 72-79, DOI: 10.1002/ejoc.200900806.

(29) Feng, X.; Iwanaga, F.; Hu, J. Y.; Tomiyasu, H.; Nakano, M.; Redshaw, C.; Elsegood, M. R.; Yamato, T. An efficient approach to the synthesis of novel pyrene-fused azaacenes. *Org. Lett.* **2013,** *15* (14), 3594-7, DOI: 10.1021/ol401438a.

(30) Xie, F.; Ran, H.; Duan, X.; Han, R.; Sun, H.; Hu, J.-Y. 1,3,5,9-Tetra(4-(1,2,2-triphenylvinyl)phenyl)pyrene (TTPE(1,3,5,9)Py): a prominent blue AIEgen for highly efficient nondoped pure-blue OLEDs. *J. Mater. Chem. C* **2020,** *8* (48), 17450-17456, DOI: 10.1039/d0tc04557h.

(31) Zhao, Z.; Chen, S.; Lam, J. W.; Lu, P.; Zhong, Y.; Wong, K. S.; Kwok, H. S.; Tang, B. Z. Creation of highly efficient solid emitter by decorating pyrene core with AIE-active tetraphenylethene peripheries. *Chem. Commun.* **2010,** *46* (13), 2221-3, DOI: 10.1039/b921451h.

(32) Crawford, A. G.; Liu, Z.; Mkhalid, I. A.; Thibault, M. H.; Schwarz, N.; Alcaraz, G.; Steffen, A.; Collings, J. C.; Batsanov, A. S.; Howard, J. A.; Marder, T. B. Synthesis of 2- and 2,7-functionalized pyrene derivatives: an application of selective C-H borylation. *Chem. Eur. J.* **2012,** *18* (16), 5022-35, DOI: 10.1002/chem.201103774.

(33) Venkataramana, G.; Dongare, P.; Dawe, L. N.; Thompson, D. W.; Zhao, Y.; Bodwell, G. J. 1,8-Pyrenylene-ethynylene macrocycles. *Org. Lett.* **2011,** *13* (9), 2240-3, DOI: 10.1021/ol200485x.

(34) Crawford, A. G.; Dwyer, A. D.; Liu, Z.; Steffen, A.; Beeby, A.; Palsson, L. O.; Tozer, D. J.; Marder, T. B. Experimental and theoretical studies of the photophysical properties of 2- and 2,7-functionalized pyrene derivatives. *J. Am. Chem. Soc.* **2011,** *133* (34), 13349-62, DOI: 10.1021/ja2006862.

(35) Allen, F. H.; Kirby, A. J. Bond length and reactivity. Variable length of the carbon-oxygen single bond. *J. Am. Chem. Soc.* **2002,** *106* (21), 6197-6200, DOI: 10.1021/ja00333a013.

(36) Feng, X.; Hu, J. Y.; Iwanaga, F.; Seto, N.; Redshaw, C.; Elsegood, M. R.; Yamato, T. Blue-emitting butterfly-shaped 1,3,5,9-tetraarylpyrenes: synthesis, crystal structures, and photophysical properties. *Org. Lett.* **2013,** *15* (6), 1318-21, DOI: 10.1021/ol4002653.

(37) Feng, X.; Tomiyasu, H.; Hu, J. Y.; Wei, X.; Redshaw, C.; Elsegood, M. R.; Horsburgh, L.; Teat, S. J.; Yamato, T. Regioselective Substitution at the 1,3- and 6,8-Positions of Pyrene for the Construction of Small Dipolar Molecules. *J. Org. Chem.* **2015,** *80* (21), 10973-8, DOI: 10.1021/acs.joc.5b02128.

(38) de Halleux, V.; Calbert, J. P.; Brocorens, P.; Cornil, J.; Declercq, J. P.; Brédas, J. L.; Geerts, Y. 1,3,6,8-Tetraphenylpyrene Derivatives: Towards Fluorescent Liquid-Crystalline Columns? *Adv. Funct. Mater.* **2004,** *14* (7), 649-659, DOI: 10.1002/adfm.200400006.

(39) Zhang, H.; Wang, Y.; Shao, K.; Liu, Y.; Chen, S.; Qiu, W.; Sun, X.; Qi, T.; Ma, Y.; Yu, G.; Su, Z.; Zhu, D. Novel butterfly pyrene-based organic semiconductors for field effect transistors. *Chem. Commun.* **2006,** (7), 755-7, DOI: 10.1039/b515433b.

(40) Sigala, P. A.; Ruben, E. A.; Liu, C. W.; Piccoli, P. M.; Hohenstein, E. G.; Martinez, T. J.; Schultz, A. J.; Herschlag, D. Determination of Hydrogen Bond Structure in Water versus Aprotic Environments To Test the Relationship Between Length and Stability. *J. Am. Chem. Soc.* **2015,** *137* (17), 5730-40, DOI: 10.1021/ja512980h.

(41) Li, S.; Lu, B.; Fang, X.; Yan, D. Manipulating Light-Induced Dynamic Macro-Movement and Static Photonic Properties within 1D Isostructural Hydrogen-Bonded Molecular Cocrystals. *Angew. Chem. Int. Ed.* **2020,** *59* (50), 22623-22630, DOI: 10.1002/anie.202009714.

(42) Li, Z.; Wang, Y.; Baryshnikov, G.; Shen, S.; Zhang, M.; Zou, Q.; Ågren, H.; Zhu, L. Lighting up solid states using a rubber. *Nat. Commun.* **2021,** *12* (1), DOI: 10.1038/s41467-021-21253-w.

(43) Tang, B. Z. Aggregology: Exploration and innovation at aggregate level. *Aggregate* **2020,** *1* (1), 4-5, DOI: 10.1002/agt2.9.

(44) Yang, J.; Fang, M.; Li, Z. Organic luminescent materials: The concentration on aggregates from aggregation‐induced emission. *Aggregate* **2020,** *1* (1), 6-18, DOI: 10.1002/agt2.2.

(45) Hatcher, P. V.; Reibenspies, J. H.; Haddon, R. C.; Li, D.; Lopez, N.; Chi, X. A polymorph of the 6,13-dichloropentacene organic semiconductor: crystal structure, semiconductor measurements and band structure calculations. *CrystEngComm* **2015,** *17* (22), 4172-4178, DOI: 10.1039/c5ce00300h.

(46) Feng, X.; Zhang, J.; Hu, Z.; Wang, Q.; Islam, M. M.; Ni, J.-S.; Elsegood, M. R. J.; Lam, J. W. Y.; Zhou, E.; Tang, B. Z. Pyrene-based aggregation-induced emission luminogens (AIEgen): structure correlated with particle size distribution and mechanochromism. *J. Mater. Chem. C* **2019,** *7* (23), 6932-6940, DOI: 10.1039/c9tc01665a.

(47) *SAINT and SADABS; Bruker AXS Inc*; Madison, Wisconsin, USA, 2009.

(48) *SHELXTL Program Package, version 5.1, Bruker AXS, Inc: ;* Madison, WI 1997.

(49) Sheldrick, G. M. *SHELXS97 and SHELXL97. Program for Crystal Structure Solution and Refinement*; University of Göttingen, Göttingen, 1997.

(50) Coventry, D. N.; Batsanov, A. S.; Goeta, A. E.; Howard, J. A.; Marder, T. B.; Perutz, R. N. Selective Ir-catalysed borylation of polycyclic aromatic hydrocarbons: structures of naphthalene-2,6-bis(boronate), pyrene-2,7-bis(boronate) and perylene-2,5,8,11-tetra(boronate) esters. *Chem. Commun.* **2005,** (16), 2172-4, DOI: 10.1039/b501778e.

Table of Contents

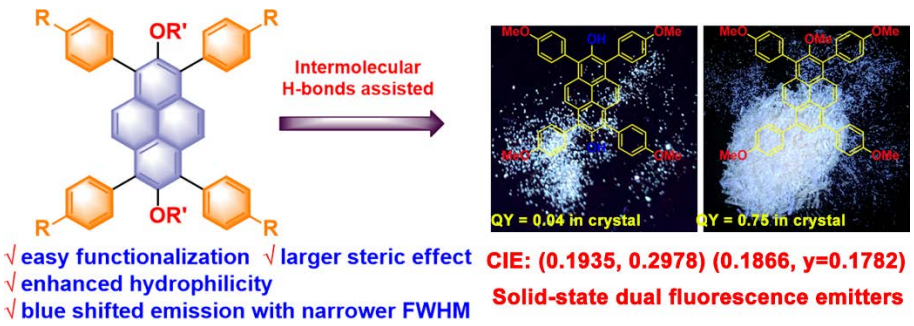

Two pyrene-based intermediates namely, 1,3,6,8-tetraaryl,2-hydroxypyrenes and 1,3,6,8-tetraaryl 2,7-dihydroxypyrenes were designed and synthesized for the preparation of novel dual-emission solid state blue emitters with mechanical force-induced enhanced emission.